International Journal of Pharmaceutics 390 (2010) 61–69

Contents lists available at ScienceDirect

International Journal of Pharmaceutics

journal homepage: www.elsevier.com/locate/ijpharm

Pharmaceutical Nanotechnology

The evidence for solid lipid nanoparticles mediated cell uptake of resveratrol

K. Teskač, J. Kristl*

University of Ljubljana, Faculty of Pharmacy, Aškerčeva 7, Ljubljana, Slovenia

ARTICLE INFO

Article history:
Received 18 February 2009
Received in revised form
18 September 2009
Accepted 3 October 2009
Available online 13 October 2009

Keywords:
Nanoparticles
Cell uptake
Resveratrol
Cell membrane
Nanomedicine
Cell cycle
Controlled release

ABSTRACT

The potential for colloidal carriers to increase drug bioavailability has spurred a renewed interest in their uptake mechanisms and movement within cells. Solid lipid nanoparticles (SLN) were used as a carrier for a promising chemopreventive drug, resveratrol (RSV). The effects of SLN, empty or loaded with RSV (SLN–RSV), on the internalization, growth, morphology, metabolic activity and genetic material of keratinocytes were compared to those of RSV in solution.

Fluorescence images clearly showed that SLN with a size below 180 nm move promptly through the cell membrane, distribute throughout the cytosol, move successively among different cellular levels and localize in the perinuclear region without inducing cytotoxicity. RSV solubility, stability and intracellular delivery were all increased by loading into SLN. The release profile of RSV showed a biphasic pattern, reflecting its distribution in SLN. RSV in solution was slightly cytotoxic. That was prevented by loading it into solid lipid nanoparticles, which preserved cell morphology. The cytostatic effect of SLN–RSV was much more expressed than that of RSV in solution. Delivery of RSV by SLN contributes to effectiveness of RSV on decreasing cell proliferation, with potential benefits for prevention of skin cancer.

1. Introduction

The development of delivery systems able to alter the biological profiles of active ingredients is of the utmost importance and requires a multidisciplinary approach. A promising strategy is the development of colloidal carriers that can transport drugs and release them at specific, desired locations. Microemulsions, nanoemulsions, polymer nanoparticles, liposomes, and solid lipid nanoparticles (SLN) composed of pharmacological acceptable excipients have all been examined for this potential (Müller et al., 2000; Marcato and Durán, 2008). SLN are composed of solid lipids and surfactants used traditionally in pharmaceutical preparations and developed originally for parenteral application. Intracellular trafficking of nanoparticles allowing an efficient cytosolic delivery system to be developed has been demonstrated (Kristl et al., 2008). This characteristic is important for the range of therapeutic targets, which could be located in the cytosol or at a deeper level within intracellular organelles, as is the case for cancer therapy (Schäfer-Korting et al., 2007).

Cancer is a disease of extreme heterogeneity. An anti-cancer agent should therefore target the multiple biochemical pathways involved in the process leading to malignancy, while having minimal side-effects and toxicity on normal tissues. It is well known that signalling pathways involved in over-proliferation and reduced differentiation can induce skin cancer. Although skin cancer is one of the few types of cancers that has become more common in recent years, it is fortunately one of the most preventable and treatable types (Horn and Gordon, 2001). It is established that signalling pathways involved in over-proliferation and reduced differentiation can induce skin cancer. Among the ever-increasing list of naturally occurring anti-carcinogenic agents, resveratrol (RSV; Fig. 1) has been extensively investigated. Resveratrol targets many components of intracellular signalling pathways, including pro-inflammatory mediators, regulators of cell survival and apoptosis, and tumour angiogenic and metastatic switches that modulate a distinct set of upstream kinases, transcription factors and their regulators (Kumar Kundua and Surha, 2008).

The potential prophylactic and therapeutic benefits of this array of activities are limited by intrinsic features that lead to low bioavailability and formulation challenges; the most serious being low water-solubility and instability (Shi et al., 2008). Carriers for RSV transport have rarely been considered (Caddeo et al., 2008), the majority of the studies being focused on molecular biology alterations caused by RSV alone (Komina and Wesierska-Gadek, 2008; Colin et al., 2008; Khan et al., 2008), but SLN have potential because of their size, hydrophobic core with hydrophilic periphery and biocompatibility (Ahlin et al., 2000; Müller et al., 2000).

Our aim was to prepare solid lipid nanoparticles (SLN) to investigate cell uptake, transport and internalization of RSV in keratinocytes. The influence of the RSV and unloaded (SLN) or with RSV-loaded SLN (SLN–RSV) on cell morphology, metabolism and genetic material was studied. Evidence is presented indicating that

* Corresponding author. Tel.: +386 1 47 69 521; fax: +386 1 47 69 512.
E-mail address: Julijana.kristl@ffa.uni-lj.si (J. Kristl).

0378-5173/$ – see front matter © 2009 Elsevier B.V. All rights reserved.
doi:10.1016/j.ijpharm.2009.10.011

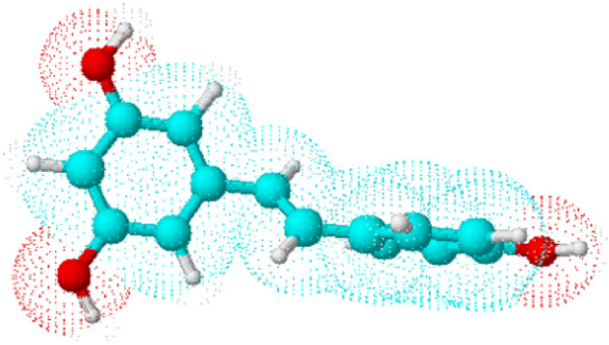

Fig. 1. Structural formula of trans-resveratrol.

SLN-mediated uptake of an active ingredient is more effective than usually assumed, compared to its passive diffusion through the cell membrane.

2. Materials and methods

2.1. Materials

Trans-Resveratrol (RSV; >99% pure) was obtained from Sigma (Germany), glyceryl behenate (Compritol 888 ATO) from Gattefosse (France), hydrogenated soya bean lecithin (Phospholipon 80H) from Natterman (Germany), and a block copolymer of polyethylene and polypropylene glycol, Lutrol F68 (Poloxamer 188) from BASF AG (Ludwigshaften, Germany). All other chemicals were of analytical grade and used as received. Water was purified by reverse osmosis. Cell culture reagents were obtained from Sigma (Germany), unless otherwise indicated.

2.2. Preparation of resveratrol samples

A 10 mM stock solution of RSV in ethanol was prepared and stored at −20 °C. Working concentration of RSV (100 μM) was obtained by dilution the stock solution with culture medium. The concentration of ethanol in the cell culture was 1:1% (v/v) that had no detectable effect on cell-viability.

2.3. Preparation of nanoparticles

Unloaded SLN were prepared by the melt-emulsification process. The lipid Compritol 888ATO (3%, w/w) and Phospholipon 80H (1%, w/w) were heated to ∼10 °C above melting point. 5 g heated aqueous solution of steric stabilizer Lutrol (0.1%, w/w) was added and the mixture stirred for 15 min at 12,000 rpm using a rotor-stator homogenizer (Omni International, Gainesville, USA) to yield a dispersion of liquid droplets in water. This dispersion was diluted with 5 g cold Lutrol solution, what cooled the lipids to form nanoparticles. In preparation procedure the temperature-sensitivity of phospholipids was considered.

RSV was loaded into SLN (SLN–RSV) by replacing 1.0% (w/w) of the Compritol by RSV. Fluorescence-labelled colloidal carriers were prepared by adding 6-coumarin dye (∼0.01%, w/w) to the lipid phase before melting. Further procedures were as those for the unlabeled nanoparticles.

2.4. Methods

2.4.1. Characterization of nanoparticles

The size and polydispersity of nanoparticles, were determined by Photon Correlation Spectroscopy (Zetasizer nano-ZS; Malvern Instrument, UK), taking the mean of three measurements. The polydispersity index indicates the width of the size distribution and has a value between 0 (monodispersity) and 1. The same instrument was used to determine the zeta potential of charged nanoparticles by observing their electrophoretic mobility in an electrical field. Zeta potential is an indicator of physical stability. An absolute value of zeta potential above 30 mV indicates high stability; below 5 mV the system is unstable.

2.4.2. RSV loading and in vitro drug release studies

RSV loading and release profile of RSV from SLN was performed by a dialysis bag method using water as dissolution medium. 2 ml of RSV solution or SLN–RSV dispersion was placed into a pre-swelled 12-kDa molecular weight cutoff (Sigma) dialysis bag with the two ends fixed by clamps. The bags were immersed in 200 ml water and agitated gently. 5 ml samples of dialysing medium were removed, with replacement, at 15 min intervals and RSV assayed by measuring the absorbance at 306 nm. The RSV released from the dialysis bag was expressed as a percentage of the original. Experiments were performed at least three times.

2.4.3. Keratinocyte culture and treatment

Cells from immortalized human keratinocyte cell line NCTC2544 (keratinocytes; ICLC, University of Genova, Italy) were cultured as adherent monolayers, routinely split 1:4 every 3–4 days, and maintained at 37 °C in a humidified atmosphere of 5% CO_2 in air. The keratinocytes were grown in Minimum Essential Medium (MEM) supplemented with 10% (v/v) fetal bovine serum (Gibco®, Invitrogen, USA), 1% (v/v) non-essential amino acids, 2 mM L-glutamine and 100 U/ml antibiotic/antimycotic.

Keratinocytes were seeded at a density of 2×10^5 cells/ml on an appropriate growing area. After 1 day (attachment phase) the cells were treated for 24 h with: (a) 100 μM of RSV solution, (b) unloaded SLN (SLN) and (c) RSV-loaded SLN (SLN–RSV) containing 100 μM RSV. The quantity of SLN was the same as for the sample SLN–RSV. Control cultures received only supplemented MEM. All experiments were done in triplicate, each condition being performed at least three times.

2.4.4. Keratinocyte metabolic activity

Metabolic activity of keratinocytes was evaluated using the MTS assay (Cell titer 96® Aqueous One Solution Cell Proliferation Assay; Promega, Madison, WI). This is based on the capacity of mitochondrial dehydrogenase to metabolize a yellow tetrazolium salt (MTS), to the dark blue formazan product. Cells were seeded in 96-well plates at 2×10^4 cells/well and treated as described above (A_S). For background values, RSV alone, unloaded or with RSV-loaded SLN at 100 μl/well were used without cells (A_{So}). Culture medium was used as a medium-only control (A_{Co}). Metabolic activity was determined by adding MTS reagent together with an electron coupling reagent (phenazine ethosulfate; PES) to the media (1:10) and incubating for 3 h at 37 °C. Absorbance was measured at 492 nm in an automated plate reader (Tecan, Mannedorf/Zürich, Switzerland). At least three independent experiments were performed. Metabolic activity of treated cells was expressed as percentage of the absorbance of untreated cells (A_C) (Eq. (1)).

$$\text{Metabolic activity}\,(\%) = \left(\frac{A_S - A_{So}}{A_C - A_{Co}}\right) \times 100 \qquad (1)$$

where A_S is the absorbance of treated cells, A_C the absorbance of untreated cells (control), A_{So} the absorbance of the test dispersion in medium without cells and A_{Co} the absorbance of the medium without cells.

2.4.5. Morphological examination of keratinocytes

Cell growth and morphology were observed using an inverted phase-contrast microscope (Olympus CKX41, Tokyo, Japan). Ker-

atinocytes incubated with test dispersions were monitored and images directly followed incubation using a digital camera (Olympus C-7070).

SLN, that passed over the cell membrane and the rates of SLN internalization with intracellular movement were monitored by live-cell imaging. Cells were plated into sterile glass chamber slides (Lab-tek Nunc, Roskilde, Denmark) and incubated overnight. Immediately after the addition of SLN labelled with 6-coumarin, the time-lapse of green fluorescence intensity was monitored on an Olympus IX81 fluorescence microscope using the 450/535 nm excitation/emission filter. Transmission micrographs and fluorescence images were collected simultaneously with the same focus settings and merged with CellR̂ Software (Olympus).

Fixed-slide preparations were established by plating keratinocytes (2×10^5 cells/ml) on square glass cover slips in six-well plates. Following 24 h incubation with test dispersions, the cells were fixed with ice-cold 4% paraformaldehyde in PBS (pH 7.4) for 10 min and permeabilized for 10 min in 0.1% Triton X-100. Nuclear morphology was visualized by using the DNA intercalating dye Hoechst 33342 (Riedel de Haen, Germany) (5 μg/ml) for 30 min in the dark and actin fibres were stained with Phalloidin–Tetramethylrhodamine B isothiocyanate (Phalloidin-TRITC; Sigma, Chemical Co., Saint Luis, ZDA) (1:40), according to the manufacturer's instructions. After that, the cover slips were removed from the wells, mounted on a slide and viewed using the following excitation/emission filter sets: 360/420 nm (Hoechst), 450/535 nm (6-coumarin), 535/635 nm (Phalloidin-TRITC). Z-stack images were generated using a constant Z-stack interval, with 60-fold objective magnification on an Olympus IX 81 fluorescence microscope using the Disc Scanning Unit (DSU) to avoid out-of-focus stray light, and processed with CellR̂ Software (all from Olympus).

2.4.6. Cell cycle analysis

Keratinocyte DNA content was determined by flow cytometry. Keratinocytes ($\sim 1 \times 10^6$) were treated for 24 h with test dispersions, and fixed with methanol at −20 °C for 2 h. The cells were re-suspended in PBS (5×10^5 cells/ml) and incubated with DNase-free RNase A (1 mg/ml; Applied Biosystems, Foster City, CA, USA) and propidium iodide (40 μg/ml; Sigma) for 1 h at room temperature in the dark. Propidium iodide fluorescence intensity (585 nm) was quantified with a FacsCalibur cytometer (BD Biosciences, San Diego, USA). To exclude aggregated cells (doublets, triplets), a single-cell gate was used and 20,000 gated events were collected for each analysis. The cell cycle profile was analyzed with CellQuest Pro software (BD Biosciences).

2.5. Statistical analysis

The values reported in the figures represent the means of experiment repeated at least three times. Data were analyzed using one-way analysis of variance (ANOVA) relative to the non-treated control. The data were expressed as means ± S.D. and a value of $P < 0.05$ was considered significant.

3. Results

3.1. Solid lipid nanoparticles as carriers for RSV delivery

The physical properties of SLN and SLN–RSV did not differ significantly. Photon correlation spectroscopy measurements gave an average hydrodynamic diameter of 180 ± 8 nm. The polydispersity index of ∼0.3 indicates a satisfactory homogeneity, and the zeta potential of −38 mV suggested physical stability. These characteristics remained almost unchanged for at least 4 weeks.

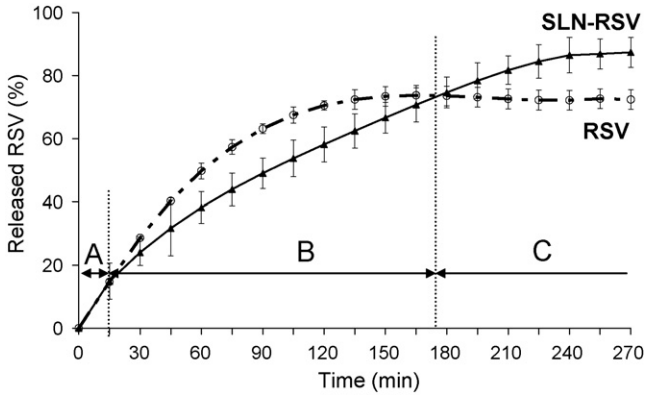

Fig. 2. Release profiles of RSV from dialysis bags, filled with RSV solution or dispersion of SLN–RSV. The concentration of free RSV in the dialysis media was followed at 15-min intervals for 3 h. Period A corresponds to release of free RSV, B to release of RSV-loaded in SLN shell and C of RSV incorporated into SLN matrix.

SLN are known to be a suitable system for drug incorporation that can prevent degradation. The lipophilic nature of RSV (log *P* of 3.3 predicted by PubChem) suggests preferential partition of RSV into the SLN sphere instead of staying in aqueous media.

Accordingly, the loading capacity was estimated from the release profile of RSV from SLN–RSV (Fig. 2). Over the first 15 min the release of RSV from RSV solution and SLN–RSV is almost identical (Fig. 2, region A). It appears that ∼15% of RSV is not bound to SLN. After 15 min there is a slower, sustained release from SLN–RSV. Various localizations of RSV are possible: the distribution in the lipid matrix, in the nanoparticle shell and adhesion to the surface. The steady release shown by area B in Fig. 2 suggests peripheral location of RSV. After the release of RSV that is adsorbed or entrapped in shell (approx. 75%), the remaining RSV incorporated into the SLN core, is released slowly over several hours (Fig. 2C).

Release of RSV is relatively rapid (Fig. 2). Surfactants, such as Lutrol, present in the aqueous phase of the dispersion enhance the solubility of RSV and thus enable its faster releasing. Further, SLN dispersions may contain other colloidal structures, such as micelles, mixed micelles and liposomes that may provide additional distribution spaces for the drug maintaining sink conditions. Finally, loading capacity is often limited by the nature of the solid lipid matrix, especially for drugs of only moderate lipophilicity. Recently, the sum of the surfaces from polar atoms in a molecule, named the "polar surface area", has been introduced to describe the interaction of a drug with the lipid of nanoparticles and its location in the nanocarrier (Ahlin et al., 2000, 2003). RSV is predominantly lipophilic (Fig. 1) but has three –OH groups with a tendency to localize at the interface in the hydrophilic area. Consequently, the physical–chemical natures of SLN and RSV both favour localization of RSV near the SLN shell, enabling ready release from the nanoparticles within 5 h.

3.2. Cell uptake of SLN and distribution studies

The intracellular delivery of SLN was followed from the first interaction between SLN–cell membrane and further uptake of SLN by the cells. Fluorescently labelled SLN was used to examine their ability to cross the cell membrane, the rate of their intracellular uptake and their distribution within the cells. The images (Fig. 3) showed that SLN rapidly crossed the membrane and the cells took up a significant fraction of the administered dose. Green fluorescence intensity can be detected inside the cells within 15 min of application (Fig. 4).

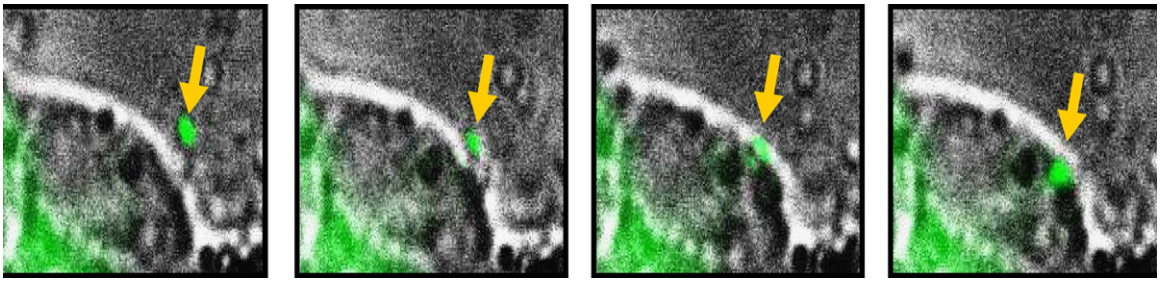

Fig. 3. Passage of a 6-coumarin-labelled nanoparticle (marked with yellow arrow) through the cell membrane. The pictures comprise merged transmission and fluorescent images taken at identical camera-focus settings at 15-s intervals. (For interpretation of the references to color in this figure legend, the reader is referred to the web version of the article.)

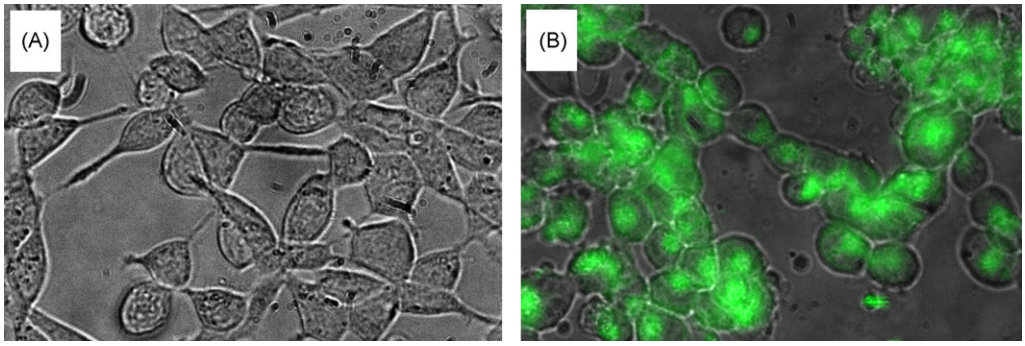

Fig. 4. Rapid increase of green fluorescence intensity in the cell cytoplasm was observed after the addition of 6-coumarin-labelled, empty SLN. The picture comprise merged transmission and fluorescent images taken at identical camera-focus settings at (A) zero time and (B) at 15 min after the addition of SLN to the cells.

The intracellular mobility of SLN is clearly indicated in Figs. 4 and 5. Initially, the nanoparticles were located on the periphery of the cells, but quickly moved towards the perinuclear region. Cell imaging of one Z-stack optical section (Fig. 5A) observed as fluorescence images at 1-min intervals showed an oscillation of green fluorescence (Fig. 5B) indicating nanoparticles traversing through the cytosol. Surprisingly, the internalized SLN do not stay in one place. It is important to note that during the experimental period of 3 days, despite constant motion of SLN within the cytosol, the cells remained completely viable, showing that SLN did not induce cytotoxicity.

3.3. Does SLN alter cell growth and morphology?

Cell morphology is a good indicator of any unusual alterations following incubation with a dispersion of colloidal particles. Fluorescence images of SLN internalization would also reveal changes in cell morphology. Keratinocytes that adopted the SLN were indistinguishable from control cells (Fig. 6).

Incubation for 24 h with 100 μM RSV resulted in a more sparsely covered growing area. However, the cell morphology after uptake of SLN–RSV depended on RSV concentration. SLN–RSV at 10 μM led to no change in cell morphology (results not shown), but at 100 μM

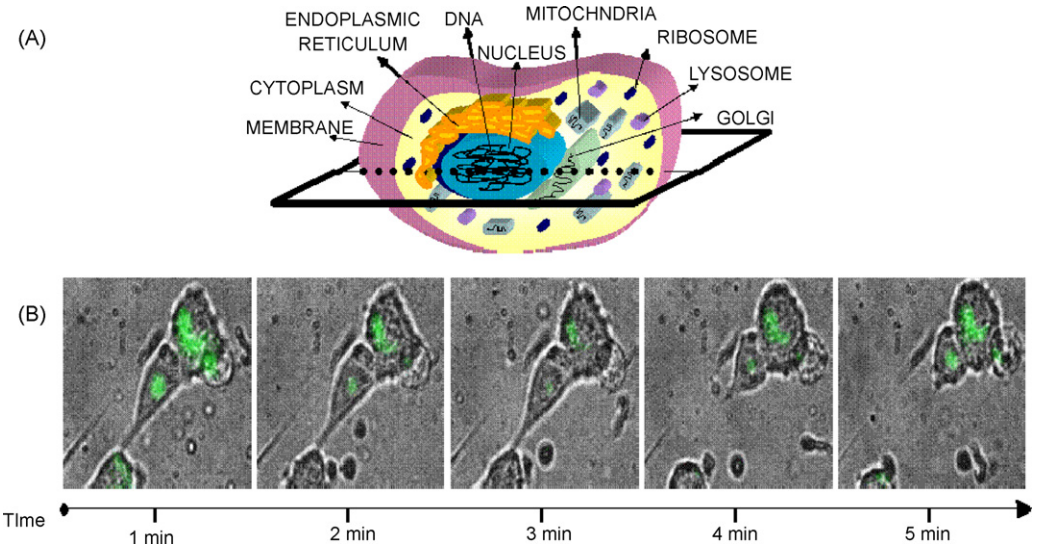

Fig. 5. Oscillation of green fluorescence due to the translocation of SLN inside the cells.(A) Illustrative presentation of one Z-stack optical section of a cell that was investigated for the fluorescence intensity. (B) Live-cell fluorescence-transmission micrographs of keratinocytes incubated for 24 h with 6-coumarin-lablled SLN, recorded at 1-min intervals at one Z-stack optical section.

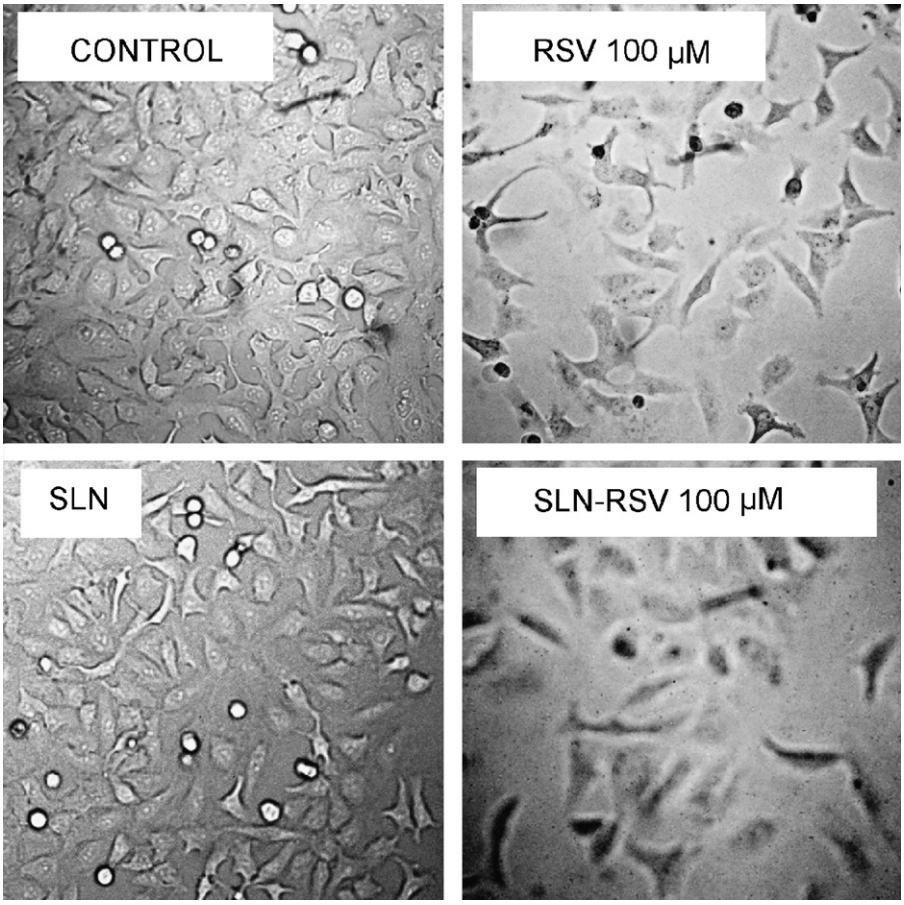

Fig. 6. Sparsely confluence of keratinocytes after exposure to RSV. Cell morphology was visualized after incubating the cells for 24 h with 100 μM RSV, in solution or loaded into SLN. To the control cells only medium was added, while SLN alone was studied by incubating the cells with the same amount of SLN as was used for SLN–RSV.

the cell number was reduced and cells were slightly enlarged (Fig. 6).

To summarize, more sparse confluence but slightly larger cells were observed when cells were incubated with SLN–RSV comparing to the RSV in solution. There are indications that SLN themselves trigger any devastative effects on keratinocytes. Therefore, when RSV is delivered by SLN, pronounced cytostatic effect is ascribed to the drug.

3.4. SLN–RSV increase cell metabolism

Mitochondrial activity, reflecting metabolic activity, was determined in order to evaluate changes in cell metabolism caused by RSV and unloaded or with RSV-loaded SLN. SLN are proven to enable intracellular transport and, due to the ability of RSV to influence various intracellular pathways, loading of RSV into SLN can also be monitored through cell metabolism, which involves many cell enzymes.

Results acquired with RSV alone showed that metabolic activity remained in the frame of the cell variability comparing to the level of control. On the contrary, when treating the cells with RSV-loaded into SLN increased metabolic activity by about 20% relative to the control was observed. SLN alone did not significantly influence metabolic activity, as is desirable in a carrier system (Fig. 7). That is in accordance with the report of Kristl et al. (2009) that RSV uptake by keratinocytes could be increased by association with a lipophilic carrier system.

What is more, the effect between free and loaded RSV is significantly different. It can be concluded that less RSV is presented intracellularly after passive diffusion (Lancon et al., 2004) comparing to SLN–RSV which accumulate intracellularly (Fig. 4). Furthermore, increased metabolic activity in a case of the

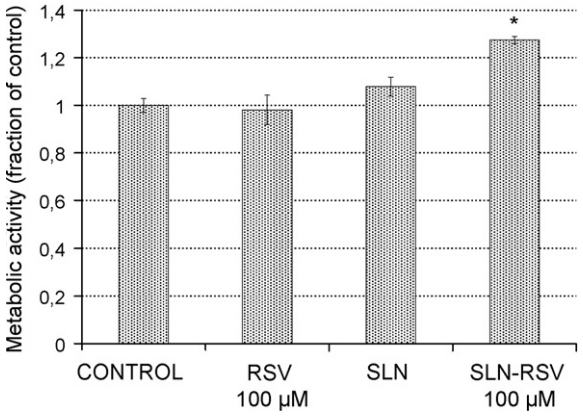

Fig. 7. Incorporation of RSV into SLN increased the metabolic activity of keratinocytes. Cell metabolic activity was assayed after incubating the cells for 24 h with 100 μM RSV in solution or loaded into SLN (SLN–RSV). To the control cells (CONTROL) only medium was added; for SLN alone (SLN), cells were incubated with the same amount of SLN as was used for SLN–RSV. Significant differences ($P < 0.05$) from control values are denoted by (*). Each value, calculated relative to control cells, represents the mean ± S.D. of at least three independent experiments.

SLN–RSV comparing to SLN is definitely ascribed to the RSV presence.

3.5. Vigorous cell cycle disturbance after exposure to SLN–RSV

Effects of SLN and RSV on the genetic material of keratinocytes were also assessed, since RSV has already been shown to influence cell cycle distribution (Komina and Wesierska-Gadek, 2008). The effects of RSV, unloaded (SLN) or with RSV-loaded SLN (SLN–RSV) were determined by measuring the fluorescence intensity of propidium iodide, which is proportional to DNA content and can be quantified by flow cytometry.

Incubation of keratinocytes with SLN for 24 h resulted in a cell cycle profile similar to that of control. Comparing these two, approximately 6% lower G1 phase, representing resting diploid cells, and a 6% increase of S-phase, representing tetraploid cells with replicated DNA, were observed. The G2/M phase was unchanged (Fig. 8).

RSV at 100 μM acted as cytostatic agent, shown as an increased G1 phase and enormous decrease of G2/M phase. S-phase of cell cycle stayed almost unchanged, which is consistent with the metabolic activity remaining at the level of control cells (Fig. 7). The consequence of reduced division is shown in Fig. 6 as a more sparsely covered cell-growing area.

Incubation with SLN–RSV moved the cells from G1 phase to S-phase of the cell cycle, accompanied by a large decrease in the G2/M phase, in which the cells are preparing to divide. Pronounced S-arrest was noticed. This was seen as increased metabolic activity (Fig. 7).

The percentage of dividing cells dropped similarly when treated with RSV or SLN–RSV. However, movement of the cells from G1 phase into S-phase, indicating increased metabolic activity, was more pronounced in the case of SLN–RSV, suggesting that intracellular transport by SLN increases the efficacy of RSV, compared to RSV alone. Consequently metabolic activity was higher in the case of SLN–RSV than in the presence of free RSV. Comparison of SLN with loaded SLN (SLN–RSV) pointed out that the marked S-arrest in the case of SLN–RSV was certainly the consequence of the RSV presence.

3.6. SLN preserved intercellular connections

RSV has been shown to affect genetic material and cell division rate (Kristl et al., 2009; Komina and Wesierska-Gadek, 2008).

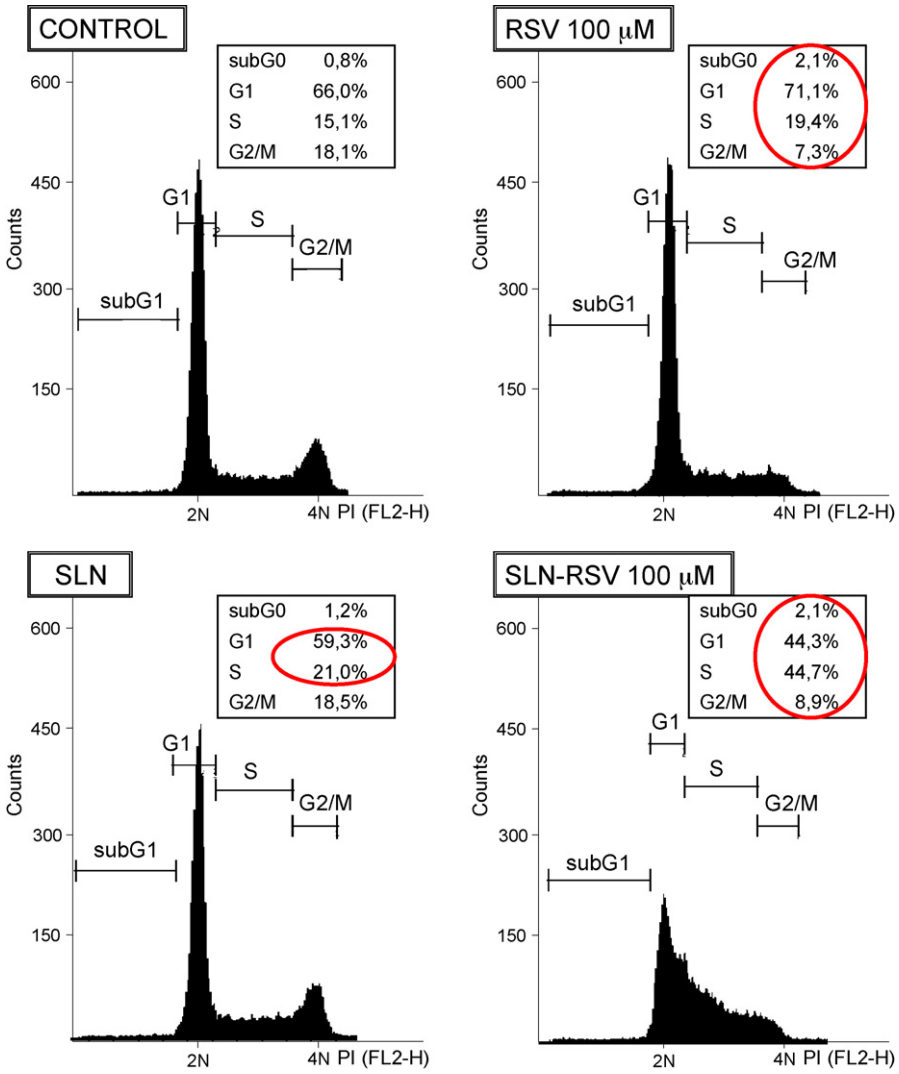

Fig. 8. Pronounced S-arrest of keratinocytes after incubation with RSV-loaded SLN. Cell cycle histograms of keratinocytes after addition of 100 μM RSV in solution (RSV) or loaded into SLN for 24 h. To the control cells only medium was added, while for SLN alone the cells were incubated with the same amount of SLN as was used for SLN–RSV. After fixation and staining of cells with propidium iodide (PI), the samples were analyzed by flow cytometry. Significant differences of cell cycle phases of treated cells compared to the control cells are encircled. 2N represents diploid cells (G1 phase) and 4N tetraploid cells (G2/M phase).

Fluorescence micrography proved intracellular localization of SLN which are concentrating around the nuclei (Fig. 4). That indicates its potential to deliver RSV to the target area for inhibition of cell division.

Obtained images of keratinocytes with SLN (green dots) show cell morphology comparable to control (Fig. 9). On the basis of the cell cycle the amount of genetic material is increased by RSV, as confirmed by the imaging. Thus larger nuclei were seen when RSV was used either in solution or as SLN–RSV. Moreover, in these cases also an arrest of the S-phase was observed, with diminished G2/M phase.

RSV at 100 μM interrupted intercellular connections and cell endings were rounded, possibly indicating the onset of necrosis, but after treatment with SLN–RSV, cell shape and general cell appearance (actin organization and nuclei shape) remained similar to the untreated, control cells (Fig. 9).

In summary sparse confluence of keratinocytes was detected after incubation the cells with RSV or SLN–RSV (Fig. 6). Metabolic activity was unaffected by RSV at 100 μM but was increased by SLN–RSV (Fig. 7). Cells division, shown as a drop of G2/M phase of a cell cycle was inhibited by RSV (Fig. 8), but delivery of RSV by SLN transposed the cells to the S-phase indicating increased metabolic activity. Morphological changes associated with necrosis seen with RSV were absent when SLN–RSV was used. The overall cytotoxicity associated with RSV was avoided by its delivery with SLN. They are rapidly uptaken and well accepted by the cells.

4. Discussion

Solid lipid nanoparticles have many features that are advantageous for nanomedicine. As a carrier system they can increase drug stability as already proven for cosmetic actives such as coenzyme Q10, ascorbyl palmitate, tocopherol and retinol (Jurkovič et al., 2003; Pardeike et al., 2009). Furthermore, the controlled release of entrapped drug is quite typical for drugs incorporated into SLN. Release profile typically shows an initial burst release followed by a prolonged release over several hours. Similar biphasic release patterns were reported for lipid nanosphere formulations by Müller et al. (2002), Ahlin et al. (2003) and Manjunath et al. (2005). They proposed that the release profile correlates with the drug loading distribution into SLN. Drug may be homogeneously distributed within the lipid matrix, concentrated in the particle shell or

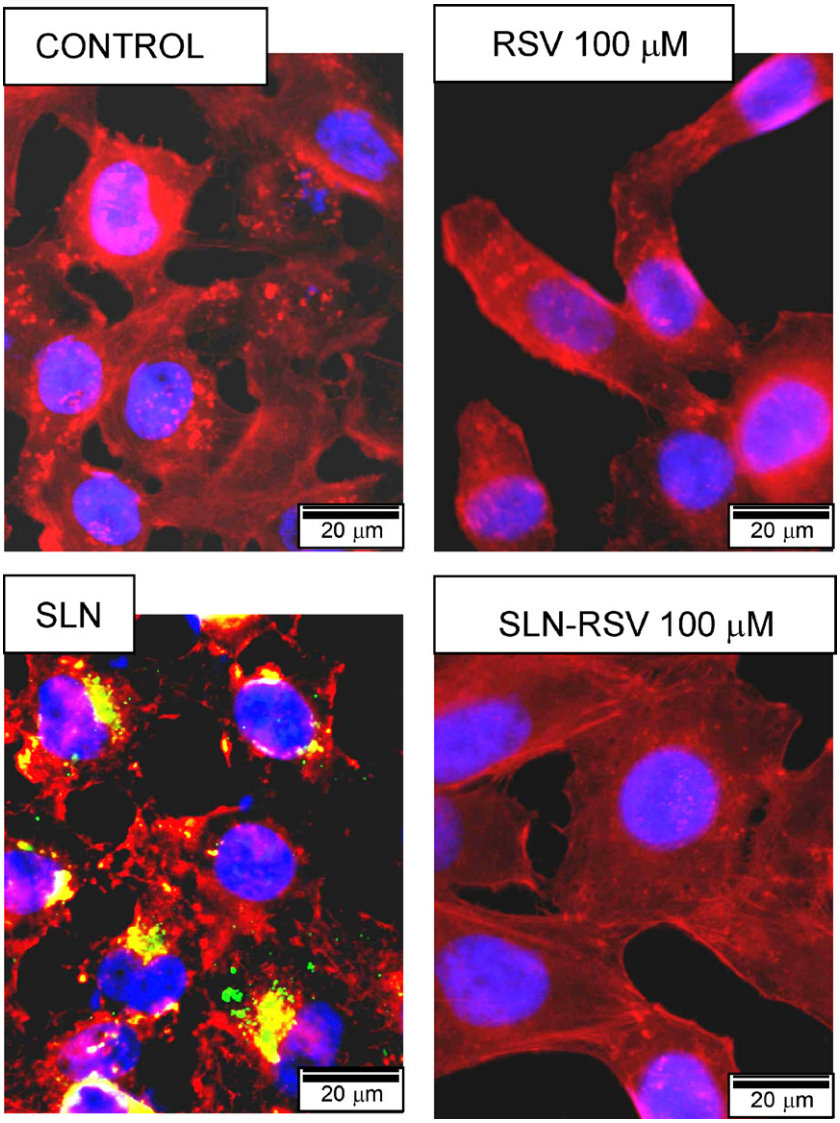

Fig. 9. Alteration of morphology after the addition of RSV, observed by fluorescence microscopy. Keratinocytes were incubated for 24 h with 100 μM RSV in solution or loaded into SLN. To the control cells only medium was added, while SLN alone (SLN) was studied by incubating the cells with 6-coumarin-lablled SLN (green) with the same amount as was used for SLN–RSV. Loaded SLN (SLN–RSV) were not fluorescently labelled. Cell nuclei were stained with Hoechst 33342 (blue), and actin fibres with TRITC (red). (For interpretation of the references to color in this figure legend, the reader is referred to the web version of the article.)

adsorbed on the particle surface. Our results suggest that about 40% is associated with the shell and is rapidly released (Fig. 2B), while the remainder, that is in the lipid matrix, being steadily released over a longer period (Fig. 2C).

So far SLN have been investigated as delivery systems mostly for cytostatic drugs that can act more efficiently comparing to the drug alone (Marcato and Durán, 2008). Although formulation procedures of SLN have been fully investigated, cell responses after their presence have been mostly overlooked.

This study clearly showed that SLN crossed the keratinocyte membrane in less than a minute (Fig. 3). They then traverse the cytoplasm and are concentrating near the nucleus (Figs. 3–5). These results are in accordance with a previous study of SLN uptake by leukocytes using electron paramagnetic resonance (Kristl et al., 2003). Matthaus et al. (2008) used Raman spectroscopy with optical microscopy to investigate the uptake mechanisms of lipid-based drug carrier systems. They found clear evidence that rate and efficiency of uptake depended on the surface properties of the nano-carriers. In our study the internalization processes were easily followed using fluorescence microscopy, combined with other advanced methods.

When SLN encounters the cell membrane several molecular interactions are possible. Various mechanisms determining its fate have been proposed. Almeida et al. (2005) considered the thermodynamic properties of membrane domains, leading to the organized movement of membrane bilayer, or the actin cytoskeleton forming cup-shaped invaginations for receptor mediated entrance (Swan, 2008). The effect of nanoparticle characteristics on the surface pressure of model membranes, can be explained on the basis of whether the interaction results in condensation of phospholipids within the membrane or their displacement into the subphase, causing membrane destabilization (Peetla and Labhasetwar, 2008).

The generally accepted model of the cell membrane model is a liquid, ordered lipid phase, with dispersed, smaller liquid-disordered domains where most proteins reside. Domain formation is a dynamic process, as some components transiently accumulate in a particular area. In our case when SLN interact with the membrane locally transient domains could be created enabling SLN cross. Distinct molecular mechanism which regulates local signal amplification in cell membrane has yet to be shown, although recent studies have shown that particle morphology influences signal-transduction mechanisms, indicating that receptor signalling is modulated by the nature of particle location at the cell surface (Swan, 2008). Cellular internalization of SLN is also ascribable to the weakness of lipid–lipid interactions, leading to a mosaic of dynamic, reversible lipid domains in the bilayer of biological membranes (Almeida et al., 2005).

Irrespective of which mechanism enables the uptake of SLN, incubation the keratinocytes for 24 h with SLN led to negligible cell damage (Fig. 6). Neither cell morphology nor cell metabolism was significantly changed (Figs. 7 and 9). Only more sensitive technique pointed on a slightly increase of S-phase in cell cycle distribution (Fig. 8).

All these results proved that SLN could be used as a carrier system to enhance the intracellular delivery of RSV. RSV has been investigated for its influence on genetic material via modulating signalling pathways on various cell types. Significant S-arrest of the cell cycle and a consequent reduction in G1 phase after RSV presence was shown for normal human fibroblasts (24 h of RSV at 30 μM) (Stivala et al., 2001), WIL2-NS non-malignant cells (24 h of RSV at 100 μM) (Lee et al., 2008), HL-60 malignant cells (24 h of RSV at 50 μM) (Komina and Wesierska-Gadek, 2008), HepG2 cells (24 h of RSV at 30 μM) (Colin et al., 2008). Since RSV has multiple actions in cell environment, especially in the periphery of the nuclear membrane (Kumar Kundua and Surha, 2008), SLN could provide benefit by delivering RSV locally, near the nuclear target site.

Our results showed that RSV preferentially inhibits the growth of keratinocytes via cell cycle modulation and so prevents the uncontrolled cell proliferation typical of cancer. Higher efficiency was achieved by delivering RSV with SLN. Cell morphology was preserved when using SLN–RSV. In contrast, RSV alone caused disappearance of intercellular connections and thus was slightly cytotoxic. RSV cytotoxicity, expressed as an induction of apoptosis, has already been reported in SW480 human colon cancer cells (Delmas et al., 2003), mouse skin tumours (Kalra et al., 2008) and malignant human pancreatic cancer cells (Sun et al., 2008). Keratinocytes, with their specialised role of protecting deeper cell layers from external perturbations, may have a very different response to RSV from these cell lines, so that our investigations on keratinocytes are prerequisite for the realization of drug carrier systems for skin cancer treatment. With respect to physical stability of the system and tolerability by the patient, SLN have proven potential also for drug application to the skin (Müller et al., 2002) and we found that SLN enable faster delivery of RSV to the target nuclear region and increase cytostatic activity of RSV. SLN prevent the cells against the cytotoxic effects associated with RSV delivered alone, what suggests the potential for development of a formulation for skin cancer therapy or prevention.

5. Conclusion

This paper clearly showed the cell uptake of RSV-loaded SLN and improved effects of RSV on cellular fate. SLN with a size below 180 nm passed rapidly through keratinocyte membranes causing no significant changes in cell morphology, metabolic activity or cell cycle. SLN are concentrated around nuclei, releasing RSV in sustained manner to express its cytostatic effect with prominent S-arrest of cell cycle and a large drop of G2/M phase.

Thus skin aggravation is reduced, the cytostatic activity of RSV is enhanced and a more successful formulation for the prevention of skin cancer is anticipated.

Acknowledgements

The authors are grateful to the ICLC-Interlab Cell. Line Collection, University of Genova (Italy) for providing the immortalized human keratinocyte cell line NCTC2544. This work was supported by the Slovenian research agency grants: P1-0189 and 312243-1/2007.

References

Ahlin, P., Šentjurc, M., Štrancar, J., Kristl, J., 2000. Localization of lipophilic substances and ageing of solid lipid nanoparticles studied by EPR. STP Pharm. Sci. 10, 125–132.

Ahlin Grabnar, P., Kristl, J., Pečar, S., Štrancar, J., Šentjurc, M., 2003. The effect of lipophilicity of spin-labelled compounds on their distribution in solid lipid nanoparticle dispersions studied by electron paramagnetic resonance. J. Pharm. Sci. 92, 58–66.

Almeida, P.F.F., Pokorny, A., Hinderliter, A., 2005. Thermodynamics of membrane domains. Biochim. Biophys. Acta 1720, 1–13.

Caddeo, C., Teskač, K., Sinico, C., Kristl, J., 2008. Effect of resveratrol incorporated in liposomes on proliferation and UV-B protection of cells. Int. J. Pharm. 363, 183–191.

Colin, D., Lancon, A., Delmas, D., Lizard, G., Abrossinow, J., Kahn, E., Jannin, B., Latruffe, N., 2008. Antiproliferative activities of resveratrol and related compounds in human hepatocyte derived HepG2 cells are associated with biochemical cell disturbance revealed by fluorescence analyses. Biochimie 90, 1674–1684.

Delmas, D., Rébé, C., Lacour, S., Filomenko, R., Athias, A., Gambert, P., Cherkaoui-Malki, M., Jannin, B., Dubrez-Daloz, L., Latruffe, N., Solary, E., 2003. Resveratrol-induced apoptosis is associated with Fas redistribution in the rafts and the formation of a death-inducing signalling complex in colon cancer cells. J. Biol. Chem. 278, 41482–41490.

Horn, M.A., Gordon, K.B., 2001. Chemoprevention of skin cancer. Cancer Treat. Res. 106, 255–282.

Jurkovič, P., Šentjurc, M., Gašperlin, M., Kristl, J., Pečar, S., 2003. Skin protection against ultraviolet induced free radicals with ascorbyl palmitate in microemulsions. Eur. J. Pharm. Biopharm. 56, 59–66.
Kalra, N., Roy, P., Prasad, S., Shukla, Y., 2008. Resveratrol induces apoptosis involving mitochondrial pathways in mouse skin tumorigenesis. Life Sci. 82, 348–358.
Khan, N., Adham, V.M., Mukhtar, H., 2008. Apoptosis by dietary agents for prevention and treatment of cancer. Biochem. Pharmacol. 76, 1333–1339.
Komina, O., Wesierska-Gadek, J., 2008. Action of resveratrol alone or in combination with roscovitine, a CDK inhibitor, on cell cycle progression in human HL-60 leukaemia cells. Biochem. Pharmacol. 76, 1554–1562.
Kristl, J., Teskač, K., Milek, M., Mlinarič-Raščan, I., 2008. Surface active stabilizer tyloxapol in colloidal dispersions exerts cytostatic effects and apoptotic dismissal of cells. Toxicol. Appl. Pharmacol. 232, 218–225.
Kristl, J., Volk, B., Ahlin, P., Gombač, K., Šentjurc, M., 2003. Interactions of solid lipid nanoparticles with model membranes and leukocytes studied by epr. Int. J. Pharm. 256, 133–140.
Kristl, J., Teskač, K., Caddeo, C., Abramović, Z., Šentjurc, M., 2009. Improvements of cellular stress response on resveratrol in liposomes. Eur. J. Pharm. Biopharm., doi:10.1016/j.ejpb.2009.06.006.
Kumar Kundua, J., Surha, Y.-J., 2008. Cancer chemopreventive and therapeutic potential of resveratrol: mechanistic perspectives. Cancer Lett. 269, 2243–2261.
Lancon, A., Delma, D., Osman, H., Thenot, J.P., Jannin, B., Latruffe, N., 2004. Human hepatic cell uptake of resveratrol: involvement of both passive diffusion and carrier-mediated process. Biochem. Biophys. Res. Commun. 316, 1132–1137.
Lee, S.K., Zhang, W., Sanderson, B.J., 2008. Selective growth inhibition of human leukaemia and human lymphoblastoid cells by resveratrol via cell cycle arrest and apoptosis induction. J. Agric. Food Chem. 56, 7572–7577.
Manjunath, K., Reddy, J.S., Venkateswarlu, V., 2005. Solid lipid nanoparticles as drug delivery systems. Methods Find. Exp. Clin. Pharmacol. 27, 127.
Marcato, P.D., Durán, N., 2008. New aspects of nanopharmaceutical delivery systems. J. Nanosci. Nanotechnol. 8, 2216–2229.
Matthaus, C., Kale, A., Chernenko, T., Torchilin, V., Diem, M., 2008. New ways of imaging uptake and intracellular fate of liposomal drug carrier systems inside individual cells, based on Raman microscopy. Mol. Pharm. 5, 287–293.
Müller, R.H., Mäder, K., Gohla, S., 2000. Solid lipid nanoparticles (SLN) for controlled drug delivery—a review of the state of the art. Eur. J. Pharm. Biopharm. 50, 161–177.
Müller, R.H., Radtke, M., Wissing, S.A., 2002. Solid lipid nanoparticles (SLN) and nanostructured lipid carriers (NLC) in cosmetic and dermatological preparations. Adv. Drug Deliv. Rev. 54, S131–S155.
Pardeike, J., Hommoss, A., Müller, R.H., 2009. Lipid nanoparticles (SLN, NLC) in cosmetic and pharmaceutical dermal products. Int. J. Pharm. 366, 170–184.
Peetla, C., Labhasetwar, V., 2008. Biophysical characterization of nanoparticle-endothelial model cell membrane interactions. Mol. Pharm. 5, 418–429.
Schäfer-Korting, M., Mehnert, W., Korting, H.C., 2007. Lipid nanoparticles for improved topical application of drugs for skin diseases. Adv. Drug Deliv. Rev. 59, 427–443.
Shi, G., Rao, L., Yu, H., Xiang, H., Yang, H., Ji, H., 2008. Stabilization and encapsulation of photosensitive resveratrol within yeast cell. Int. J. Pharm. 349, 83–93.
Swan, A.Joel., 2008. Shaping cups into phagosomes and macropinosomes. Nature Review. Mol. Cell Biol. 9, 639–649.
Stivala, L.A., Savio, M., Carafoli, F., Perucca, P., Bianchi, L., Maga, G., Forti, L., Pagnoni, U.M., Albini, A., Prosperi, E., Vannini, V., 2001. Specific structural determinants are responsible for the antioxidant activity and the cell cycle effects of resveratrol. J. Biol. Chem. 276, 22586–22594.
Sun, W., Wang, W., Kim, J., Keng, P., Yang, S., Zhang, H., Liu, C., Okunieff, P., Zhang, L., 2008. Anti-cancer effect of resveratrol is associated with induction of apoptosis via a mitochondrial pathway alignment. Adv. Exp. Med. Biol. 614, 179–186.